ISSN 0915-633X

NATIONAL INSTITUTE FOR FUSION SCIENCE

A Possibility of π^- Meson Production by a Low Energy Electron Bunch and Positive Ion Bunch

J. Uramoto

(Received – Feb. 22, 1994)

NIFS-277

Apr. 1994

RESEARCH REPORT
NIFS Series

NAGOYA, JAPAN

A Possibility of π^- Meson Production by a Low Energy Electron Bunch and Positive Ion Bunch

Jōshin URAMOTO

National Institute of Fusion Science,

Nagoya 464-01, Japan

Abstract

A low energy electron beam ($\leq$ 1200 eV) is injected perpendicularly to a uniform magnetic field, together with a low energy positive ion beam which is stopped electrically. On these magnetic mass analyses (using the uniform magnetic field), two peaks of secondary electron to the beam collector appear at two analyzing magnetic field intensities which correspond to two relations of μ^- muon (the mass $m_1 = 207\ m_e$ and the charge $q_1 = e$) and π^- meson (the mass $m_2 = 273\ m_e$ and the charge $q_2 = e$, where m_e and e are mass and charge of electron). We consider that the π^- meson may be produced by a coherent interaction between the magnetically bunched beam electrons and the electrically bunched beam ions, and that the negative muon μ^- may be produced through the decay of π^- meson.

Keywords: π^- meson, negative muon μ^-, bunched beam electron, bunched beam ion

We have already reported[1] that the negative muonlike particle $\overset{\circ}{\mu}^-$ appears when a low energy electron beam accompanying positive ion beam are injected perpendiculary to a uniform magnetic field. However, the direct production of negative muon μ^- from the electrons violates the lepton number conservation law. Therefore, we must reexamine the previous experimental results[1] of negative muonlike particle production. In this report, we improved an electrical insulation of the beam collector with respect to the mass analyzer body and noted dependences on the beam collector bias voltage more precisely.

Schematic diagrams of the experimental apparatus are shown in Fig. 1 and Fig. 2. The initial or first electron beam (F.E.B.) is stopped critically in front of the entrance slit S by an electrical potential of the decelerator D connected to the cathode of the electron gun. Next, a neutral gas is introduced into the first electron beam region and a plasma is produced through ionization of the gas. Then, positive ions of the plasma are accelerated in front of S while a positive ion beam with an energy corresponding to the first electron beam acceleration voltage V_A, is injected into the magnetic field region through S. Moreover, the stopped beam electrons are reaccelerated electrically toward the gap between two magnetic poles (N) and (S) through S, while the injected ion beam is decelerated electrically and stopped in the gap. The electrically reaccelerated electrons are injected perpendicularly to the magnetic field (B_M) and bunched in cyclotron motions of small radius.

As shown in Fig. 2, the above magnetic system is used as a mass analyzer (M.A.) of 90° type when the beam collector B.C. is arranged. The analyzing curvature radius r is 4.3 cm. It should be noted that the bias voltage V_S of the beam collector is positive with respect to the mass analyzer in order to reject a positive ion current and draw back the secondary electrons.

A fringe magnetic field distribution of the analyzing magnetic field B_M under a magnetic coil current of 1A, is shown in Fig. 3 for two different metal plates as the entrance plate (decelerator D) of Fig. 1 and Fig. 2. In this experiment, the iron (Fe) plate is used and the fringe magnetic field is much reduced.

The distribution of electrically applied potential are shown in Fig. 4. The first electron beam from the electron gun is perfectly reflected in front of the entrance slit S of the magnetic mass analyzer (M.A.) while a plasma is produced by a gas (air) ionization. Then, a positive ion beam is

injected into M.A. through the slit S and the second electron beam is produced by reacceleration of the plasma electrons. It should be noted that the injected positive ion beam (i_2) is decelerated and stopped electrically, and that the second electron beam (e_2) suffers a magnetron (cyclotron) motion in the uniform magnetic field (which is used as the analyzing magnetic field of M.A.). As a result, both the electron beam and positive ion beam will be bunched within the small space at the entrance X of the uniform magnetic field.

Thus, we can expect a coherent interaction between the bunched electrons and positive ions.

Dependences of negative current I^- to the beam collector B.C. on the analyzing magnetic field B_M are shown in Fig. 5 and Fig. 6 for various first electron beam acceleration voltage V_A under two positive bias voltage V_S of the beam collector $V_S = 80V$ and $V_S = 100V$. Here, when $V_S = 80V$, we find that an analyzing relation of the negative muon μ^- is satisfied for each peak of negative current I^-, if we assume that the effective acceleration voltage V_E is twice of the first electron beam acceleration voltage V_A. That is, the following relation is found: From the analyzing magnetic field B_M where the negative current shows a peak, the curvature radius r of the mass analyzer and the effective acceleration voltage V_E, we can estimate the mass m of the negatively charge particle by,

$$m = \frac{Ze\,(B_M r)^2}{2V_E}$$

$$= \frac{8.8 \times 10^{-2}\, Z\,(B_M r)^2\, m_e}{V_E}, \quad \text{..... (1)}$$

where e is the electron charge, B_M is in gauss unit, r is in cm unit, V_E is in volt unit and m_e is the electron mass and Z is the charge number. For the curvature radius $r = 4.3$ cm of this mass analyzer, the Eq. (1) is rewritten by

$$m = \frac{1.63\, Z\, B_M^2}{V_E} m_e. \quad \text{..... (2)}$$

From the experimental conditions in Fig. 5, we obtain $m = m_1 \approx 207\, m_e$ for $V_E = 2\, V_A$, assuming that $Z = 1$. This experimental result is similar to the previous one.[1] However, when $V_S = 100V$ (Fig. 6), we find another kind of negative current peak with the ordinary negative

muonlike peak.[1] That is, from the experimental conditions for the another peak in Fig. 6, we obtain (assuming that the charge $q_2 = e$) $m_2 \approx 290\ m_e$ using the analyzing magnetic field B_M of another peak of negative current I^- and Eq. (2). This mass m_2 is very near the mass ($\approx 273\ m_e$) of π^- meson (within a few percent).

This second peak of I^- greatly depends on the positive bias voltage V_S as shown in Fig. 7. The threshold voltage of V_S is between 80V and 100V under the first electron acceleration voltage $V_A = 400V$ and the neutral pressure (air) in the electron beam region $P \approx 6 \times 10^{-6}$ Torr. Similarly, the second peak of I^- depends on the neutral pressure P in the electron beam region as shown in Fig. 8 (A) and Fig. 8 (B), which does not depend on a current of the first electron beam as shown in Fig. 9.

Finally, the variations of the negative current characteristic are shown for two neutral gases H_2 or H_e in Fig. 10. We find that both the first and the second peak position of the analyzing magnetic fields do not vary for various gases. For H_2 gas, the third peak of I^- appears near 3 times larger value of the analyzing magnetic field, compared with the first peak of negative muon. Obviously, this third peak of I^- shows negative hydrogen ion H^-. We can consider that the H^- ions are produced in the "plasma" region in Fig. 4, and that their initial energies are neglisibly small at the entrance slit S. Then, we find from the experimental results (Fig. 10), that the H^- ions are accelerated by an effective potential $V_E = 2\ V_A$ (twice of the initially applied voltage V_A between S and X in Fig. 1 and Fig. 2) as shown in Fig. 4. That is, the electrons and H^- ions from S, will be accelerated by both the initially applied V_A (between S and X) and an additional potential ($+V_A$) generated by stopping an positive ion beam (of supplied gas) which is accelerated initially by V_A between the "plasma" region and S. Thus, the secondary produced μ^- and π^- will be also accelerated by the effective potential V_E.

If the π^- meson is produced in the above experiments and the μ^- muon generates through the decay of the π^- meson, the violation of "lepton number conservation law" in the previous experiments[1] (a direct production from the electrons), is avoidable.

The bias voltage dependences of the beam collector for the detection of π^- or μ^-, may be explaned from the energy distribution for generation of secondary electrons by the π^- or μ^-. That is, the secondary electron energy for the π^- may be higher than that for the μ^-. Thus, in order

to draw back the higher energy secondary electrons, the higher positive bias voltage of the beam collector may be required for the detection of the π^- meson.

To produce one π^- meson, an energy of $E_\pi = 139.6$ MeV or 2.2×10^{-11} Joule is required for the electron beam. Thus, a net current I_t^- (μA) of the produced π^- meson is estimated from an effective electron beam power W_{ef} (W) injected into the mass analyzer, if the kinetic energy of π^- is neglected, by

$$I_t^- \approx \frac{eW_{ef}}{E_\pi}$$

$$= 7.1 \times 10^{-3}\ W_{ef}\ (\mu A). \quad \cdots\cdots (3)$$

When the π^- meson is detected at the beam collector position, the cyclotron radius of π^- is equal to the analyzing radius $r = 4.3$ cm of the mass analyzer. At this magnetic field intensity of the mass analyzer, the electron cyclotron radius is estimated to be about $r_e = 0.26$ cm from the mass ratio of $m_2/m_e \approx 273$, if the π^- and the electron are accelerated at the same potential ($2\ V_A$). Then, the flight time of π^- from the production position X to the beam collector B.C. is $t_\pi = (2\pi r/4)/v_\pi$, where v_π is the velocity of π^-. During this flight time t_π, the number of the electron cyclotron motions are estimated to be $t_\pi/(2\pi r_e/v_e) = (1/4)\ (r/r_e)\ (v_e/v_\pi)$, where v_e is the electron velocity and $(2\pi r_e/v_e) = t_e$ means a time of one electron cyclotron motion. As the $(r/r_e)\ (v_e/v_\pi)$ is equal to the mass ratio $m_2/m_e = 273$, the number of electron cyclotron motion is determined to be about 68 times.

Here, if the cyclotron motions of about 68 times of the beam electrons inside the mass analyzer is considered as an energy multiplication due to a kind of confinement, Eq. (3) is rewritten by,

$$I_t^- \approx 5.5 \times 10^{-1}\ W_b\ (\mu A)$$

$$= 5.5 \times 10^{-7}\ I_b V_b\ (\mu A), \quad \cdots\cdots (4)$$

where W_b is an usual electron beam power (W unit), and I_b and V_b are the injected electron beam current (μA) and the effective electron beam acceleration voltage (V).

When the injected electron beam current is about 50 μA and the effective acceleration voltage is about 1000V, we obtain $I_t^- \approx 0.03\ \mu A$ from Eq. (4). On the other hand, the apparent negative

current to the beam collector is around 3.0 μA. That is, the discrepancy ratio (I^-/I_t^-) is around 100. We consider that this discrepancy between the net current I_t^- and the apparent current I^- is due to the negative current of the secondary electrons generated by the π^- through the gas ionization or the impacts with the beam collector surface.

Inversely, we can consider that a very weak generation of π^- by a small power of the low energy electron beam, is observed clearly from the multiplied apparent current.

As a reason for which the μ^- is easily detected, we can point out that the life time of π^- is much shorter (2.6×10^{-8} sec) than that of μ^- (2.2×10^{-6} sec). That is, the flight time from the generating place of π^- to the beam collector is ranging from 8.7×10^{-8} sec to 3.5×10^{-8} sec for the effective acceleration voltage V_E = 400V ~ 2400V. Thus, the π^- may decay into the μ^- during the flight time.

The electron beam current injected into M.A. through the slit S, is measured, which is around 50 μA at a total electron current (to the electron gun anode) I_A = 1.0 mA. The electron beam current hardly depends on the acceleration voltage V_A of the first electron beam and the neutral gas pressure P (1×10^{-5} Torr ~ 1×10^{-4} Torr) in the first electron beam region. The injected electron beam current density is estimated to be about $j_{eo} = e\, n_{eo}\, v_{eo} = 1.7 \times 10^{-4}$ A/cm^2, where e, n_{eo} and v_{eo} are electron charge, an initially injecting electron density and an initial electron velocity. Thus, the initial electron density n_{eo} is determined to be about $n_{eo} \approx 10^6$/cc at I_A = 1.0 mA and V_A = 400V.

Similarly, the positive ion (N_2^+ for air) beam current injected through the slit S, is measured, which is about 0.1 μA (for the neutral gas pressure P = 1×10^{-5} Torr) and about 0.5 μA (for P = 1×10^{-4} Torr) at I_A = 1.0 mA. The positive ion beam current greatly depends on the neutral gas pressure P and much increases with P, while it does not depend on V_A. The injected positive ion beam current density is estimated to be about $j_{io} = e\, n_{io}\, v_{io} = 3.3 \times 10^{-7}$ A/cm^2 (for P = 1×10^{-5} Torr) and 1.7×10^{-6} A/cm^2 (for P = 1×10^{-4} Torr), where n_{io} and v_{io} are an initially injecting positive ion density and an initial positive ion velocity. Thus, the initial positive ion density n_{io} is determined to be about $n_{io} = 3 \times 10^5$/cc (for P = 1×10^{-4} Torr) and $n_{io} = 1.5 \times 10^6$/cc (for P = 1×10^{-4} Torr), at I_A = 1.0 mA and V_A = 400V.

For the analyzing magnetic field B_M and the first acceleration voltage V_A where the negative

current I^- shows each peak, the electron cyclotron radius is $r_{ce} \approx 0.3$ cm (at μ^- peak) or $r_{ce} \approx 0.26$ cm (at π^- peak). Therefore, if the injected electron beam motion is stopped magnetically, the electron number density n_e abruptly increases in the small space, which can be expressed by a continuity law of the electron current. That is,

$$n_e = \frac{n_{oe}\, v_{oe}}{v_e}, \quad \text{..... (5)}$$

$$v_e \rightarrow o \text{ (magnetically)},$$

where v_e is an electron velocity in the direction of initial electron beam.

On the other hand, the injected positive ion beam motion is stopped electrically as understood from the electrical potential ($+|V_A|$) of the mass analyzer body and the slit potential (o). Therefore, the positive ion number density n_i in the entrance of the magnetic poles (N) and (S) in Fig. 1, abruptly increases in the same place of the electron bunch. That is,

$$n_i = \frac{n_{oi}\, v_{oi}}{v_i}, \quad \text{..... (6)}$$

$$v_i \rightarrow o \text{ (electrically)},$$

where v_i is a positive ion velocity in the direction of initial positive ion beam.

From these discussions, we may consider a coherent interaction[1] between the bunched beam electrons and positive ions, which may produce the π^- meson. Then, the average effective potential V_E which accelerates the produced π^- meson, is determined to be $V_E = 2V_A$ by a macroscopic potential difference between the electron bunch and the positive ion bunch.

In conclusion, the μ^- muon may be produced through the decay of π^- meson.

Reference

1. J. Uramoto, *NIFS Report No.* **266** (1993).

Fig. 1 and Fig. 2: Schematic diagrams of the experimental apparatus.

F: Filament as electron emitter. K: Cathode of electron gun. A: Anode of electron gun. V_A: Initial electron acceleration voltage. I_A: Total negative current. F.E.B.: First electron beam. G: Neutral gas. D: Decelerator of F.E.B. S: Entrance slit (3 mm × 10 mm). Ins: Insulator. I.B.: Ion beam. S.E.B.: Second electron beam. e: Electrons with cyclotron motions. μ^-: Negative muon. (M.A.): Mass analyzer. Fe: Iron. C: Magnetic Coil. (N): North pole of electro-magnet. (S): South pole. B_M: Analyzing magnetic field. B.C.: Beam collector. I^-: Negative current to B.C. V_S: Bias voltage of B.C. with respect to mass analyzer body. S.P.: Secondary plasma inside (M.A.). X: Entrance of uniform magnetic field. i: Ion bunch. π^-: Negative π meson.

Fig. 3 Fringe magnetic field distribution.

B_M: Analyzing magnetic field of (M.A.). B_O: Uniform magnetic field inside (M.A.). X: End of uniform magnetic field. S: Entrance slit position. Fe: Magnetic field distribution in a case using iron plate as D in Fig. 1. Cu: Magnetic field distribution in a case using copper plate as D in Fig. 1.

Fig. 4 Applied electrical potential distribution.

V: Electrical potential. V_A: Initial potential (voltage) of electron gun anode. V_E: Effective potential for μ^- (negative muon) and π^- (negative π meson). e_0: Initial electrons from electron gun cathode. e_1: First electron beam. e_2: Second electron beam. i_1: Positive ion beam from plasma. i_2: Second positive ion beam. e–B: Electron bunch due to magnetic cyclotron motion. i–B: Positive ion bunch due to electrical retardation. K: Cathode position of electron gun. A: Anode position of electron gun. S: Slit position of mass analyzer. X: Entrance position of analyzing uniform magnetic field. $+V_A$:Additional potential generated by stopping the positive ion beam. (H^-): Negative hydrogen ion accelerated by the effective potential $V_E = 2\ V_A$.

Fig. 5 Dependences of the negative beam collector current I^- on the analyzing magnetic field B_M under various initial electron acceleration voltages V_A. The positive beam collector bias voltage $V_S = 80V$.

(1): $V_A = 100V$. (2): $V_A = 200V$. (3): $V_A = 400V$. (4): $V_A = 800V$. (5): $V_A = 1200V$.

The neutral gas pressure (air) is 6×10^{-6} Torr in the first electron beam region. μ^-: (means negative muon). The total anode current $I_A = 1.5$ mA.

Fig. 6 Dependences of the negative beam collector current I^- on the analyzing magnetic field B_M under various initial electron acceleration voltages V_A. The positive beam collector bias voltage $V_S = 100V$.

(1): $V_A = 100V$. (2): $V_A = 200V$. (3): $V_A = 400V$. (4): $V_A = 800V$. (5): $V_A = 1200V$.

The neutral gas pressure (air) is 6×10^{-6} Torr in the first electron beam region. μ^-: (means negative muon). The total anode current $I_A = 1.5$ mA. π^- (means negative π meson).

Fig. 7 Dependences of the negative beam collector current I^- on B_M under various bias voltages V_S of the beam collector at $V_A = 400V$.

A: $V_S = 60V$. B: $V_S = 80V$. C: $V_S = 100V$. D: $V_S = 120V$. E: $V_S = 150V$. F: $V_S = 200V$.

The neutral gas pressure (air) is 6×10^{-6} Torr in the first electron beam region. The total anode current $I_A = 1.5$ mA. μ^-: (means negative muon). π^-: (means negative π meson).

Fig. 8 (A) Dependences of I^- on B_M under various pressure P (air) in the first electron beam region at $V_A = 400V$, $V_S = 80V$ and $I_A = 1.5$ mA.

A: $P = 6 \times 10^{-6}$ Torr. B: $P = 3 \times 10^{-5}$ Torr. C: $P = 1.2 \times 10^{-4}$ Torr.

Fig. 8 (B) Dependences of I^- on B_M under various pressure P (air) in the first electron beam region (F.E.B.) at $V_A = 200V$ and $I_A = 1.5$ mA.

A: $P = 6 \times 10^{-6}$ Torr. B: $P = 5 \times 10^{-5}$ Torr. C: $P = 1 \times 10^{-4}$ Torr.

Fig. 9 Dependences of I^- on B_M under various total current I_A to electron gun anode at $V_A = 400V$ and $V_S = 80V$, and pressure in F.E.B. = 6×10^{-6} Torr.

A: $I_A = 0.5$ mA. B: $I_A = 1.5$ mA. C: $I_A = 3$ mA.

Fig. 10 Dependences of I^- on B_M under various gases (H_e and H_2) at $V_A = 200V$, $V_S = 100V$, $I_A = 1.0$ mA, P (H_e) = 2.8×10^{-4} Torr, and P (H_2) = 3×10^{-4} Torr in F.E.B.

μ^-: negative muon. π^-: negative π meson. H^-: negative hydrogen ion.

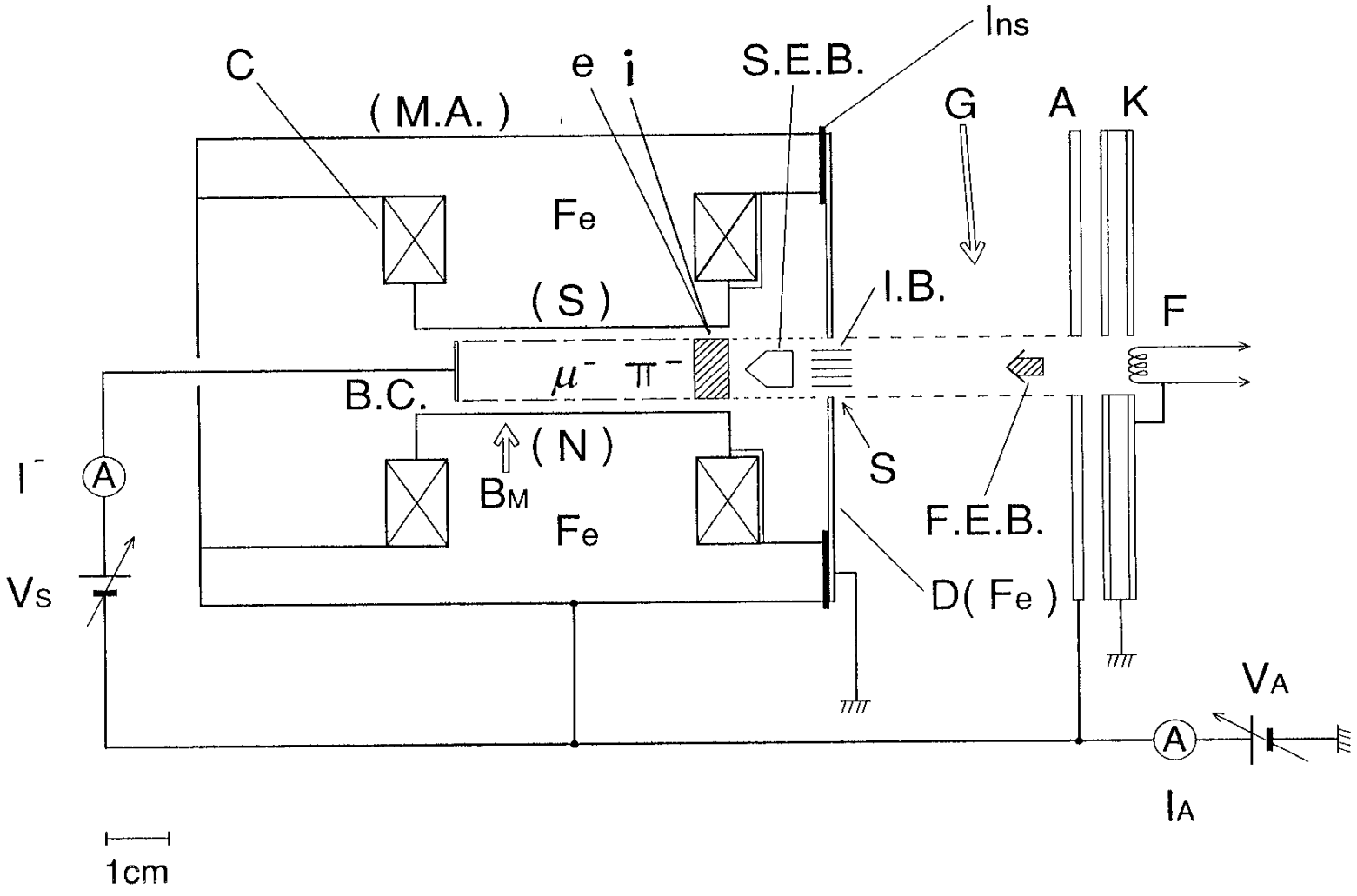

Fig. 1

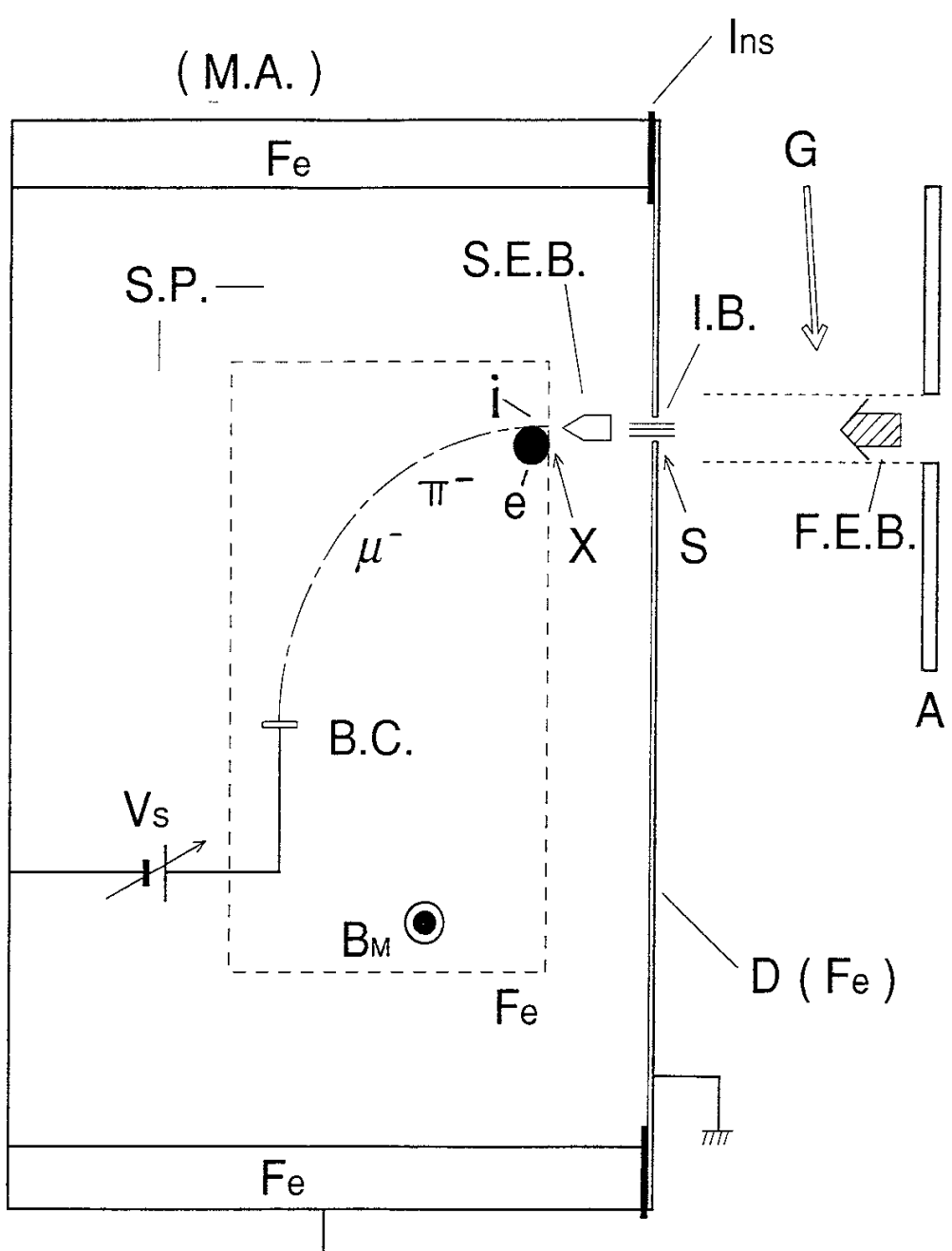

Fig. 2

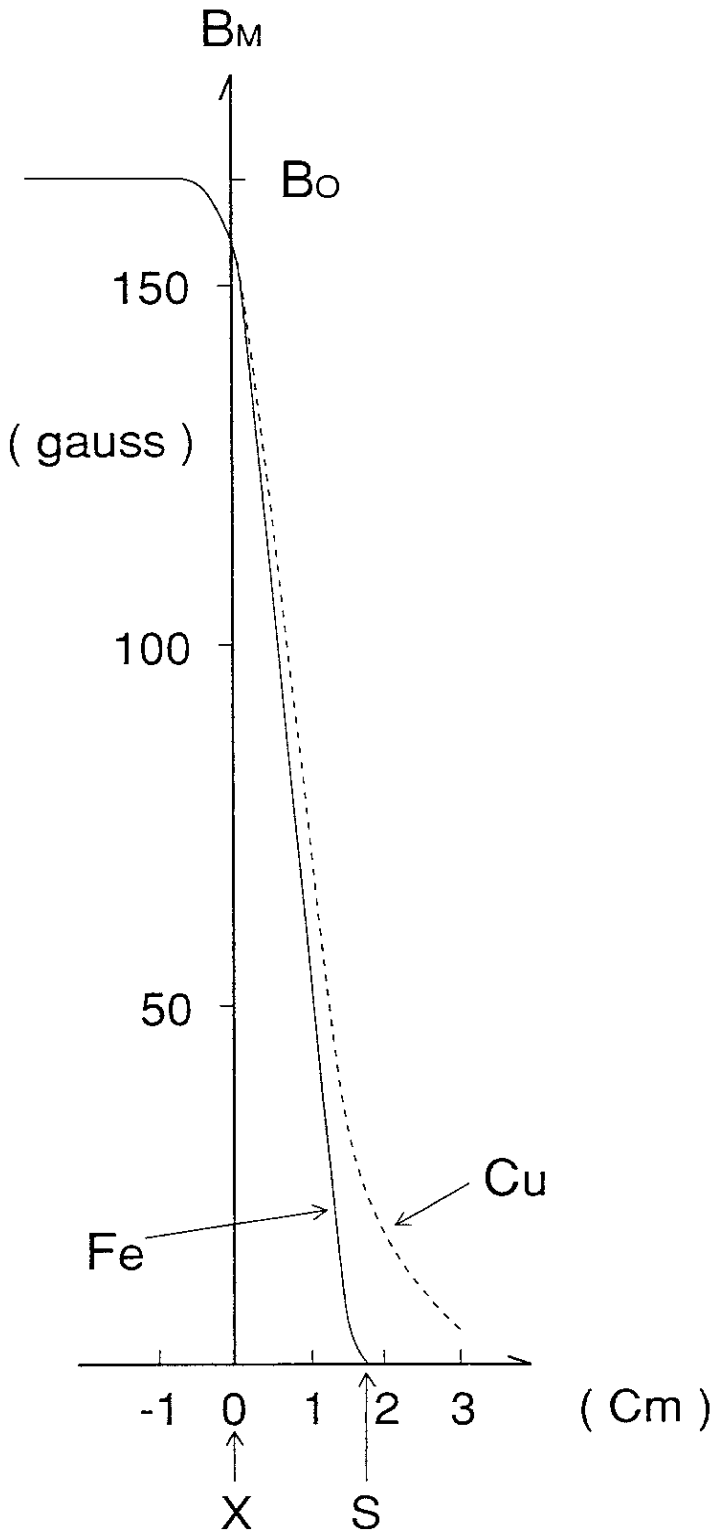

Fig. 3

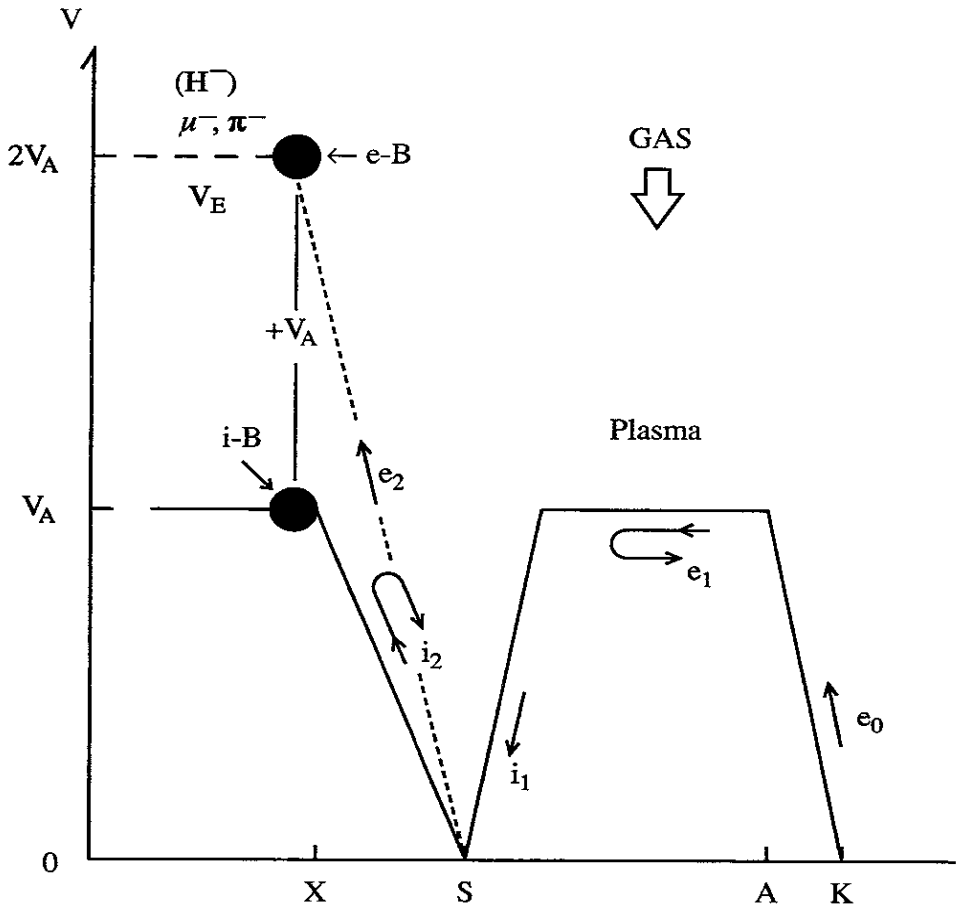

Fig. 4

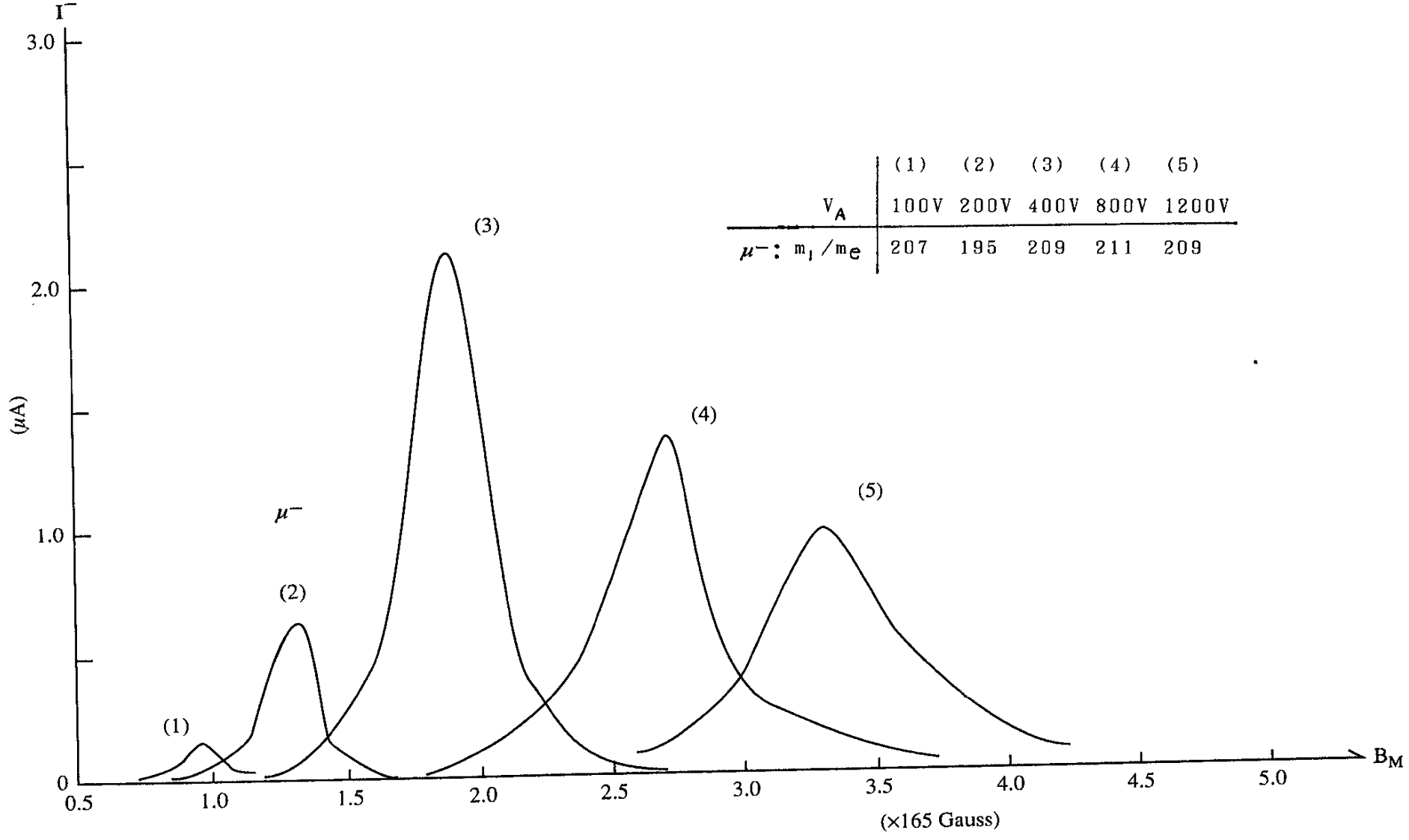

	(1)	(2)	(3)	(4)	(5)
V_A	100V	200V	400V	800V	1200V
μ^-: m_μ / m_e	207	195	209	211	209

Fig. 5

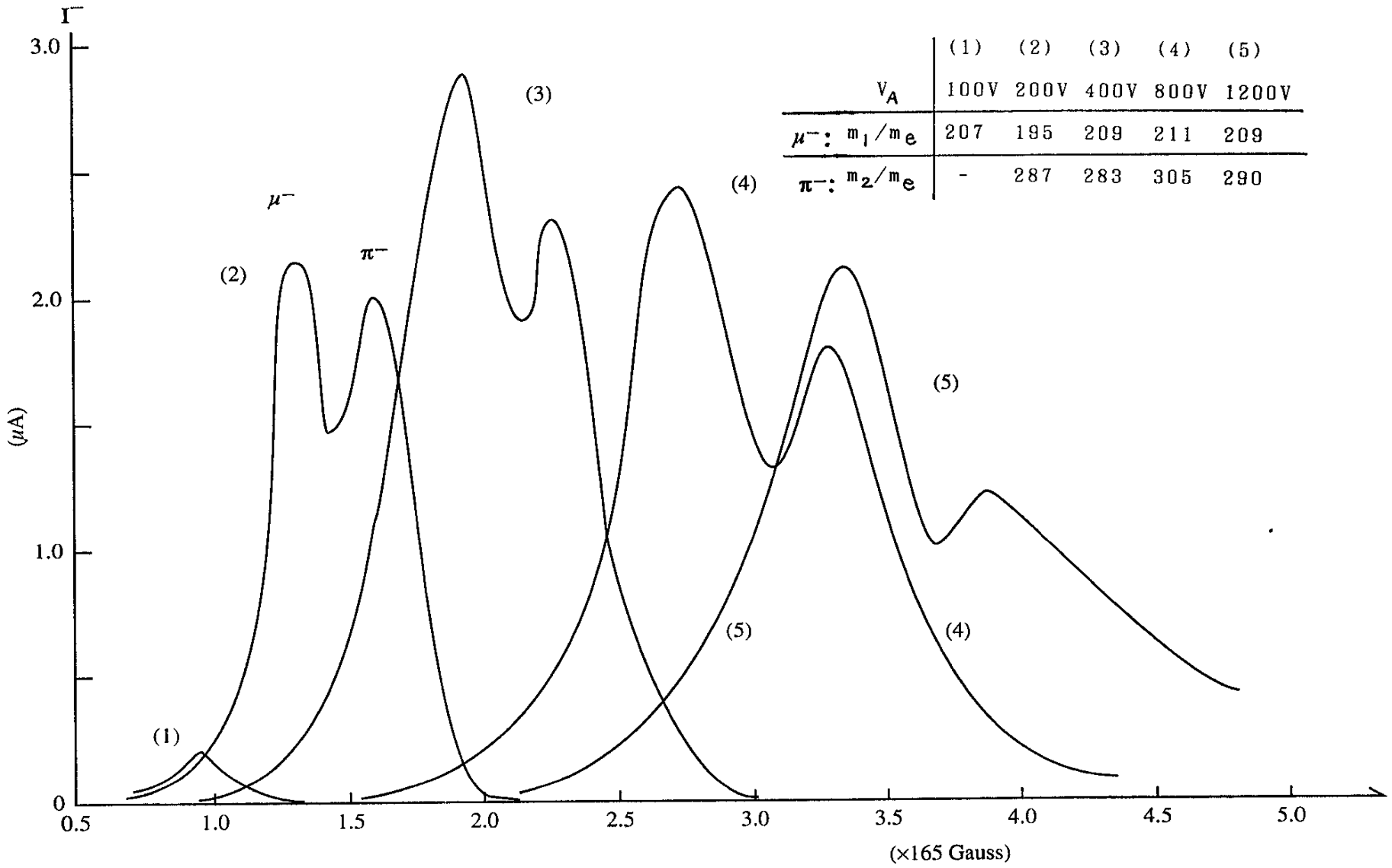

	(1)	(2)	(3)	(4)	(5)
V_A	100V	200V	400V	800V	1200V
μ^-: m_1/m_e	207	195	209	211	209
π^-: m_2/m_e	-	287	283	305	290

Fig. 6

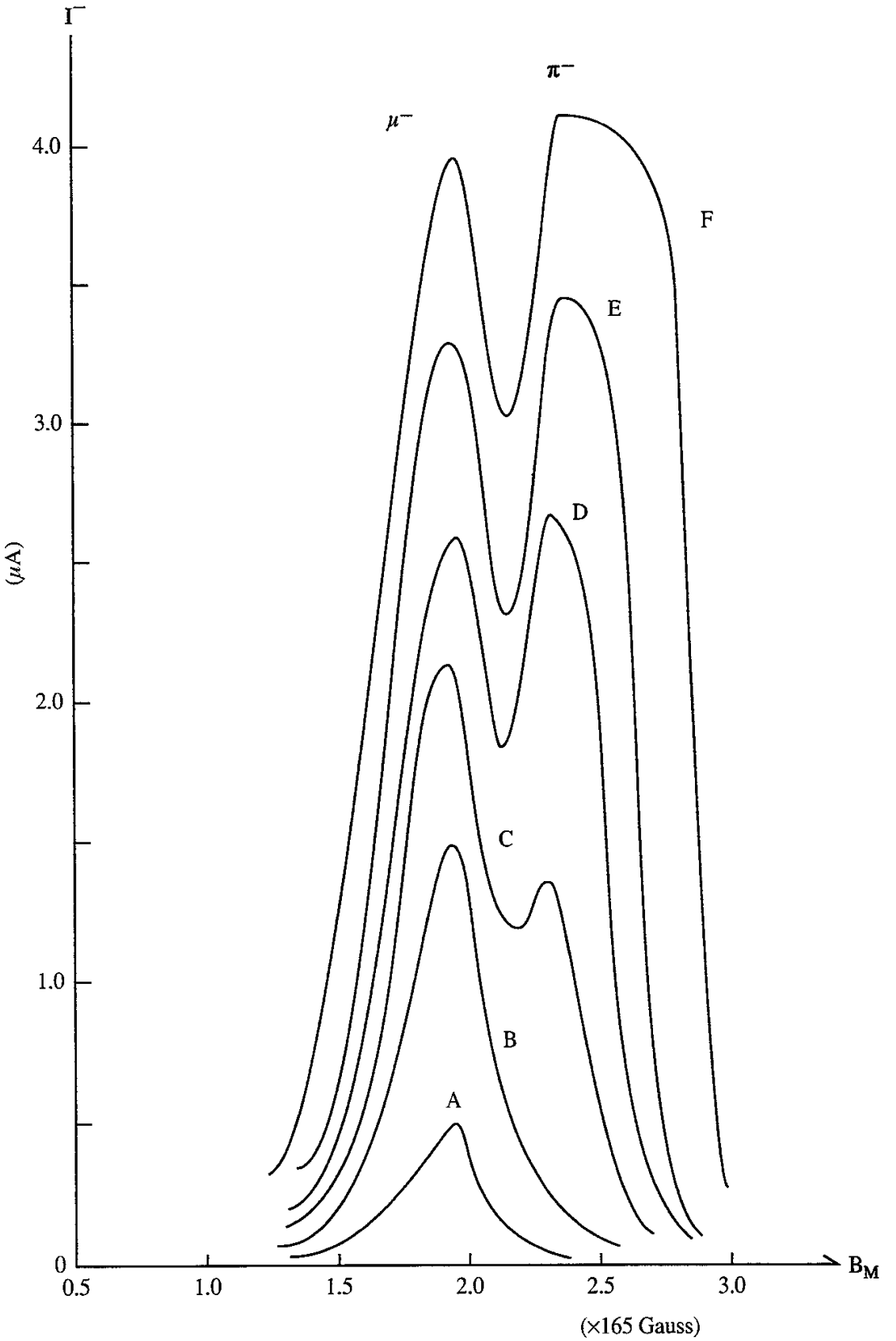

Fig. 7

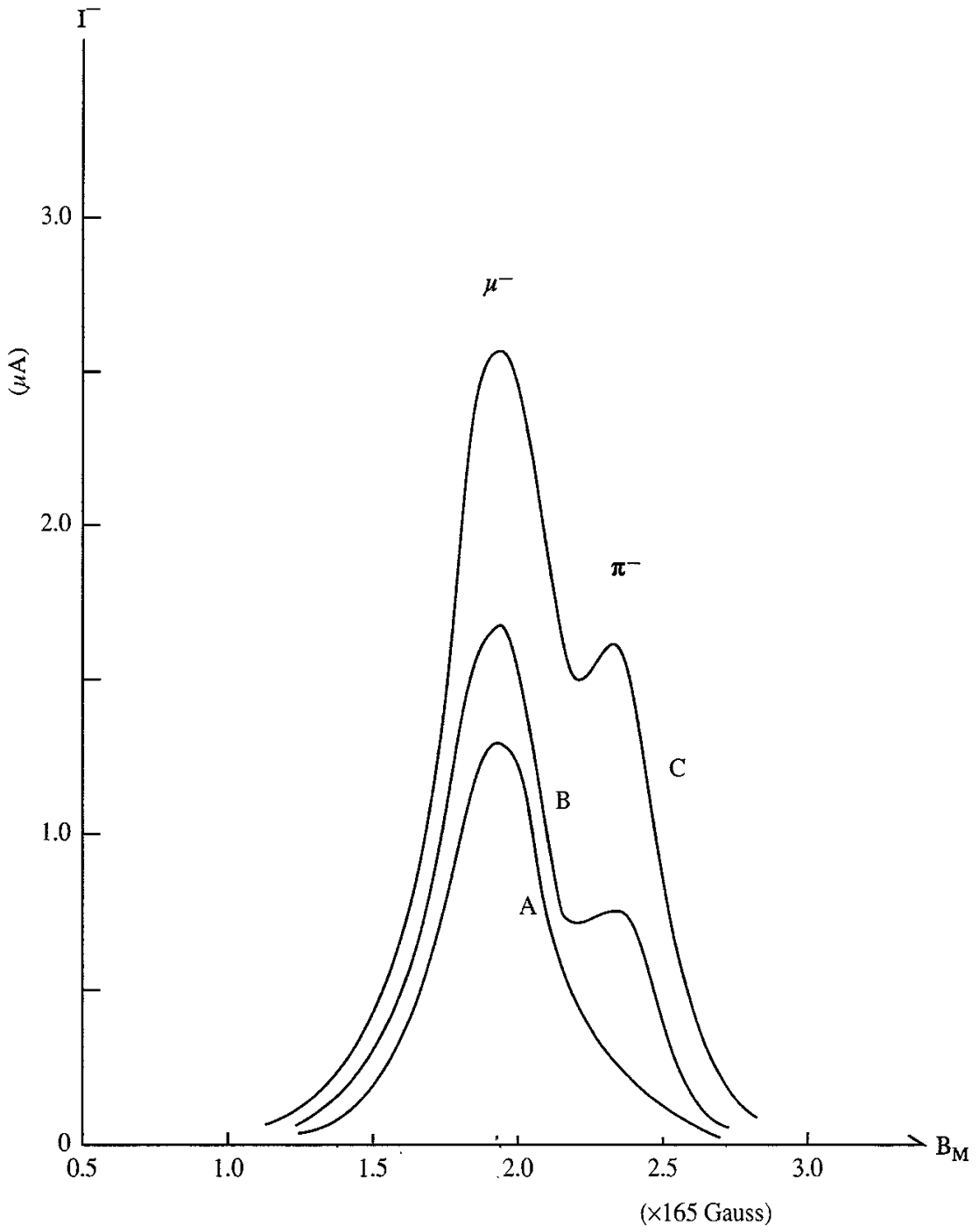

Fig. 8 (A)

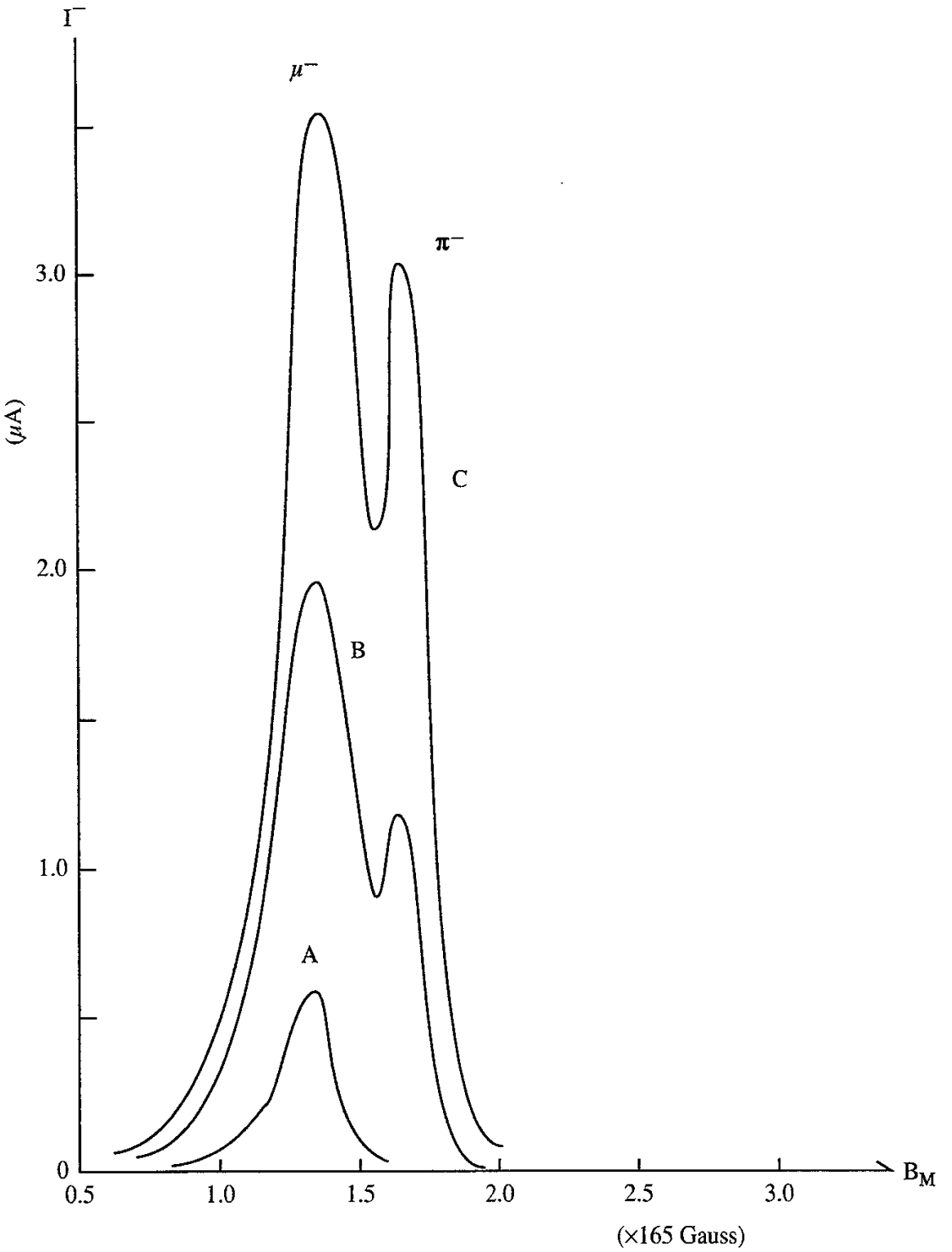

Fig. 8 (B)

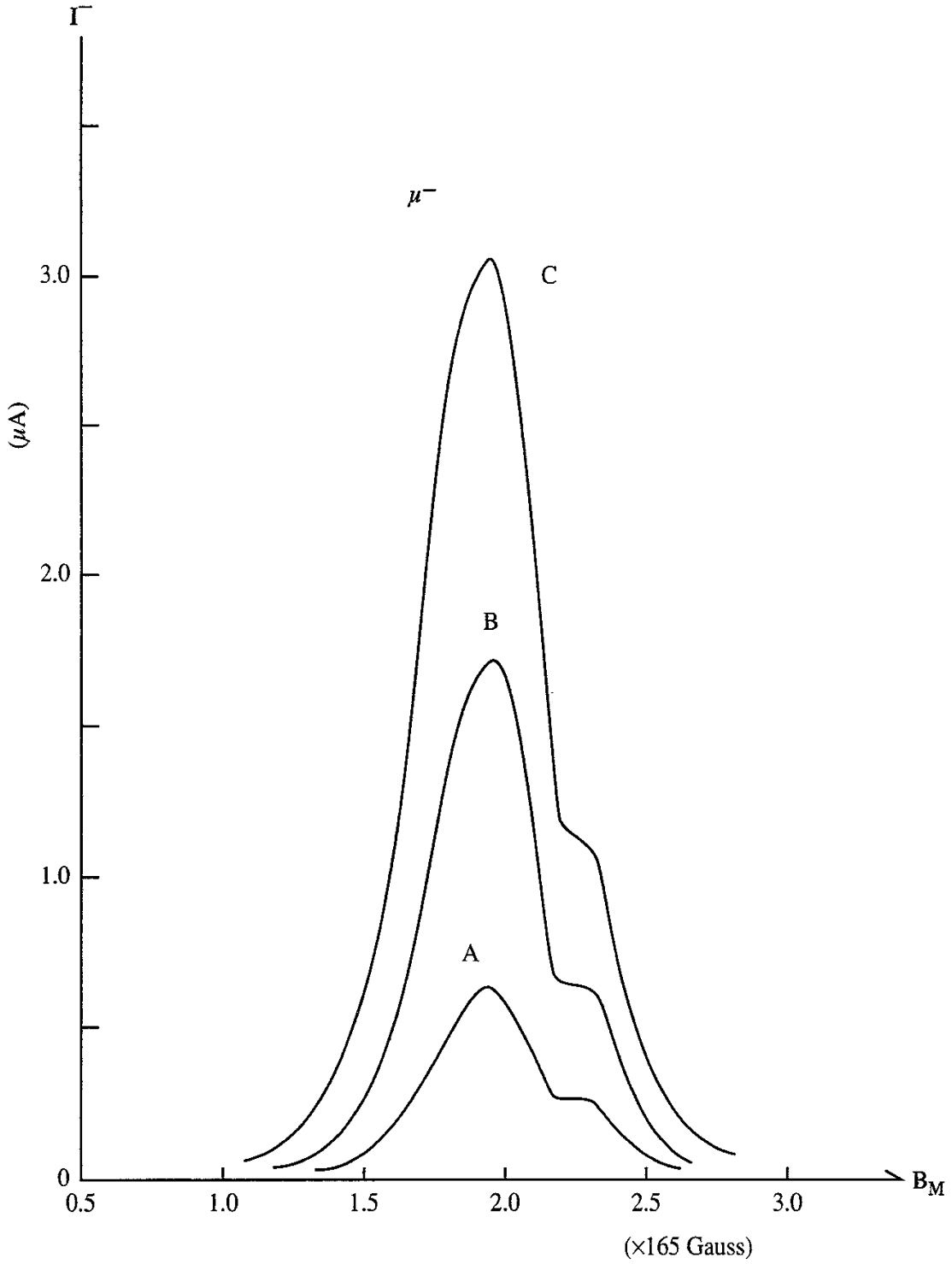

Fig. 9

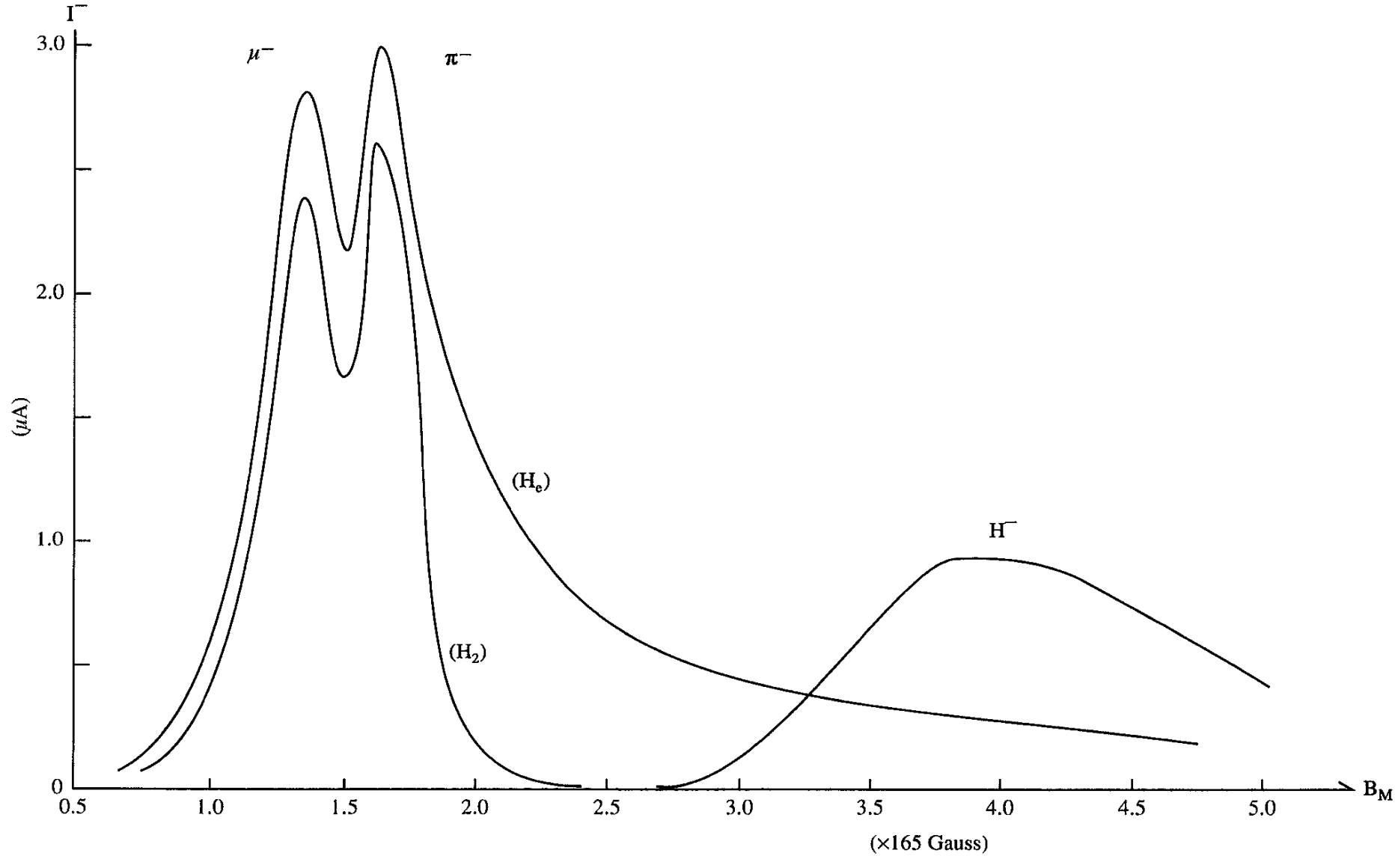

Fig. 10

Recent Issues of NIFS Series

NIFS-230 H. Idei, K. Ida, H. Sanuki, H. Yamada, H. Iguchi, S. Kubo, R. Akiyama, H. Arimoto, M. Fujiwara, M. Hosokawa, K. Matsuoka, S. Morita, K. Nishimura, K. Ohkubo, S. Okamura, S. Sakakibara, C. Takahashi, Y. Takita, K. Tsumori and I. Yamada, *Transition of Radial Electric Field by Electron Cyclotron Heating in Stellarator Plasmas;* June 1993

NIFS-231 H.J. Gardner and K. Ichiguchi, *Free-Boundary Equilibrium Studies for the Large Helical Device*, June 1993

NIFS-232 K. Itoh, S.-I. Itoh, A. Fukuyama, H. Sanuki and M. Yagi, *Confinement Improvement in H-Mode-Like Plasmas in Helical Systems*, June 1993

NIFS-233 R. Horiuchi and T. Sato, *Collisionless Driven Magnetic Reconnection*, June 1993

NIFS-234 K. Itoh, S.-I. Itoh, A. Fukuyama, M. Yagi and M. *Azumi, Prandtl Number of Toroidal Plasmas;* June 1993

NIFS-235 S. Kawata, S. Kato and S. Kiyokawa , *Screening Constants for Plasma;* June 1993

NIFS-236 A. Fujisawa and Y. Hamada, *Theoretical Study of Cylindrical Energy Analyzers for MeV Range Heavy Ion Beam Probes;* July 1993

NIFS-237 N. Ohyabu, A. Sagara, T. Ono, T. Kawamura and O. Motojima, *Carbon Sheet Pumping;* July 1993

NIFS-238 K. Watanabe, T. Sato and Y. Nakayama, *Q-profile Flattening due to Nonlinear Development of Resistive Kink Mode and Ensuing Fast Crash in Sawtooth Oscillations;* July 1993

NIFS-239 N. Ohyabu, T. Watanabe, Hantao Ji, H. Akao, T. Ono, T. Kawamura, K. Yamazaki, K. Akaishi, N. Inoue, A. Komori, Y. Kubota, N. Noda, A. Sagara, H. Suzuki, O. Motojima, M. Fujiwara, A. Iiyoshi, *LHD Helical Divertor;* July 1993

NIFS-240 Y. Miura, F. Okano, N. Suzuki, M. Mori, K. Hoshino, H. Maeda, T. Takizuka, JFT-2M Group, K. Itoh and S.-I. Itoh, *Ion Heat Pulse after Sawtooth Crash in the JFT-2M Tokamak;* Aug. 1993

NIFS-241 K. Ida, Y.Miura, T. Matsuda, K. Itoh and JFT-2M Group, *Observation of non Diffusive Term of Toroidal Momentum Transport in the JFT-2M Tokamak;* Aug. 1993

NIFS-242 O.J.W.F. Kardaun, S.-I. Itoh, K. Itoh and J.W.P.F. Kardaun,

Discriminant Analysis to Predict the Occurrence of ELMS in H-Mode Discharges; Aug. 1993

NIFS-243 K. Itoh, S.-I. Itoh, A. Fukuyama,
Modelling of Transport Phenomena; Sep. 1993

NIFS-244 J. Todoroki,
Averaged Resistive MHD Equations; Sep. 1993

NIFS-245 M. Tanaka,
The Origin of Collisionless Dissipation in Magnetic Reconnection; Sep. 1993

NIFS-246 M. Yagi, K. Itoh, S.-I. Itoh, A. Fukuyama and M. Azumi,
Current Diffusive Ballooning Mode in Seecond Stability Region of Tokamaks; Sep. 1993

NIFS-247 T. Yamagishi,
Trapped Electron Instabilities due to Electron Temperature Gradient and Anomalous Transport; Oct. 1993

NIFS-248 Y. Kondoh,
Attractors of Dissipative Structure in Three Disspative Fluids; Oct. 1993

NIFS-249 S. Murakami, M. Okamoto, N. Nakajima, M. Ohnishi, H. Okada,
Monte Carlo Simulation Study of the ICRF Minority Heating in the Large Helical Device; Oct. 1993

NIFS-250 A. Iiyoshi, H. Momota, O. Motojima, M. Okamoto, S. Sudo, Y. Tomita, S. Yamaguchi, M. Ohnishi, M. Onozuka, C. Uenosono,
Innovative Energy Production in Fusion Reactors; Oct. 1993

NIFS-251 H. Momota, O. Motojima, M. Okamoto, S. Sudo, Y. Tomita, S. Yamaguchi, A. Iiyoshi, M. Onozuka, M. Ohnishi, C. Uenosono,
Characteristics of D-^{3}He Fueled FRC Reactor: ARTEMIS-L, Nov. 1993

NIFS-252 Y. Tomita, L.Y. Shu, H. Momota,
Direct Energy Conversion System for D-^{3}He Fusion, Nov. 1993

NIFS-253 S. Sudo, Y. Tomita, S. Yamaguchi, A. Iiyoshi, H. Momota, O. Motojima, M. Okamoto, M. Ohnishi, M. Onozuka, C. Uenosono,
Hydrogen Production in Fusion Reactors, Nov. 1993

NIFS-254 S. Yamaguchi, A. Iiyoshi, O. Motojima, M. Okamoto, S. Sudo, M. Ohnishi, M. Onozuka, C. Uenosono,
Direct Energy Conversion of Radiation Energy in Fusion Reactor, Nov. 1993

NIFS-255 S. Sudo, M. Kanno, H. Kaneko, S. Saka, T. Shirai, T. Baba,
Proposed High Speed Pellet Injection System "HIPEL" for Large Helical Device
Nov. 1993

NIFS-256 S. Yamada, H. Chikaraishi, S. Tanahashi, T. Mito, K. Takahata, N. Yanagi, M. Sakamoto, A. Nishimura, O. Motojima, J. Yamamoto, Y. Yonenaga, R. Watanabe,
Improvement of a High Current DC Power Supply System for Testing the Large Scaled Superconducting Cables and Magnets; Nov. 1993

NIFS-257 S. Sasaki, Y. Uesugi, S. Takamura, H. Sanuki, K. Kadota,
Temporal Behavior of the Electron Density Profile During Limiter Biasing in the HYBTOK-II Tokamak; Nov. 1993

NIFS-258 K. Yamazaki, H. Kaneko, S. Yamaguchi, K.Y. Watanabe, Y.Taniguchi, O.Motojima, LHD Group,
Design of Central Control System for Large Helical Device (LHD); Nov. 1993

NIFS-259 K. Yamazaki, H. Kaneko, S. Yamaguchi, K.Y. Watanabe, Y.Taniguchi, O.Motojima, LHD Group,
Design of Central Control System for Large Helical Device (LHD); Nov. 1993

NIFS-260 B.V.Kuteev,
Pellet Ablation in Large Helical Device; Nov. 1993

NIFS-261 K. Yamazaki,
Proposal of "MODULAR HELIOTRON': Advanced Modular Helical System Compatible with Closed Helical Divertor; Nov. 1993

NIFS-262 V.D.Pustovitov,
Some Theoretical Problems of Magnetic Diagnostics in Tokamaks and Stellarators; Dec. 1993

NIFS-263 A. Fujisawa, H. Iguchi, Y. Hamada
A Study of Non-Ideal Focus Properties of 30° Parallel Plate Energy Analyzers; Dec. 1993

NIFS-264 K. Masai,
Nonequilibria in Thermal Emission from Supernova Remnants; Dec. 1993

NIFS-265 K. Masai, K. Nomoto,
X-Ray Enhancement of SN 1987A Due to Interaction with its Ring-like Nebula; Dec. 1993

NIFS-266 J. Uramoto
A Research of Possibility for Negative Muon Production by a Low Energy Electron Beam Accompanying Ion Beam; Dec. 1993

NIFS-267 H. Iguchi, K. Ida, H. Yamada, K. Itoh, S.-I. Itoh, K. Matsuoka, S. Okamura, H. Sanuki, I. Yamada, H. Takenaga, K. Uchino, K. Muraoka,
The Effect of Magnetic Field Configuration on Particle Pinch Velocity in Compact Helical System (CHS); Jan. 1993

NIFS-268 T. Shikama, C. Namba, M. Kosuda, Y. Maeda,
Development of High Time-Resolution Laser Flash Equipment for Thermal Diffusivity Measurements Usting Miniature-Size Specimens; Jan. 1994

NIFS-269 T. Hayashi, T. Sato, P. Merkel, J. Nührenberg, U. Schwenn,
Formation and 'Self-Healing' of Magnetic Islands in Finite-β Helias Equilibria; Jan. 1994

NIFS-270 S. Murakami, M. Okamoto, N. Nakajima, T. Mutoh,
Efficiencies of the ICRF Minority Heating in the CHS and LHD Plasmas; Jan. 1994

NIFS-271 Y. Nejoh, H. Sanuki,
Large Amplitude Langmuir and Ion-Acoustic Waves in a Relativistic Two-Fluid Plasma; Feb. 1994

NIFS-272 A. Fujisawa, H. Iguchi, A. Taniike, M. Sasao, Y. Hamada,
A 6MeV Heavy Ion Beam Probe for the Large Helical Device; Feb. 1994

NIFS-273 Y. Hamada, A. Nishizawa, Y. Kawasumi, K. Narihara, K. Sato, T. Seki, K. Toi, H. Iguchi, A. Fujisawa, K. Adachi, A. Ejiri, S. Hidekuma, S. Hirokura, K. Ida, J. Koong, K. Kawahata, M. Kojima, R. Kumazawa, H. Kuramoto, R. Liang, H. Sakakita, M. Sasao, K. N. Sato, T. Tsuzuki, J. Xu, I. Yamada, T. Watari, I. Negi,
Measurement of Profiles of the Space Potential in JIPP T-IIU Tokamak Plasmas by Slow Poloidal and Fast Toroidal Sweeps of a Heavy Ion Beam; Feb. 1994

NIFS-274 M. Tanaka,
A Mechanism of Collisionless Magnetic Reconnection; Mar. 1994

NIFS-275 A. Fukuyama, K. Itoh, S.-I. Itoh, M. Yagi and M. Azumi,
Isotope Effect on Confinement in DT Plasmas; Mar. 1994

NIFS-276 R.V. Reddy, K. Watanabe, T. Sato and T.H. Watanabe,
Impulsive Alfven Coupling between the Magnetosphere and Ionosphere, Apr.1994